ACS OMEGA

Open Access

http://pubs.acs.org/journal/acsodf

Article

Fluorimetric Detection of Vapor Pollutants with Diketopyrrolopyrrole Polymer Microcavities

Laura Magnasco, Andrea Lanfranchi, Martina Martusciello, Heba Megahd, Giovanni Manfredi, Paola Lova, Beata Koszarna, Daniel T. Gryko, and Davide Comoretto*

Cite This: *ACS Omega* 2024, 9, 42375−42385

Read Online

ACCESS | Metrics & More | Article Recommendations | Supporting Information

ABSTRACT: The increasing prevalence and detrimental effects of volatile organic compounds are driving the need for selective on-site sensors that do not require complex sampling or instrumentation. Broadband selective sensors exhibiting selectivity based on their distinct response mechanism is becoming of increasing technological relevance in both industrial and urban settings. In this context, we propose a label-free sensor based on a polymeric planar microcavity embedded with a fluorescent organic dye, designed to detect various pollutants in the vapor phase. The sensor consists of alternating layers of cellulose acetate and poly(*N*-vinylcarbazole) and contains a polystyrene defect layer doped with a quadrupolar diketopyrrolopyrrole. Both the structural properties of the polymer microcavity and the dye in the defect layer contribute to the sensor's response to analytes, creating a dual-probe system where a single photonic element translates chemical signals into optical signals, namely, transmission and fluorescence spectral variations. The discrimination capability of the photonic structure arises from the physicochemical interactions between the analytes and the polymer components. To validate our approach, we evaluate the sensor's response to four distinct volatile molecules and investigate the mechanisms influencing the optical response.

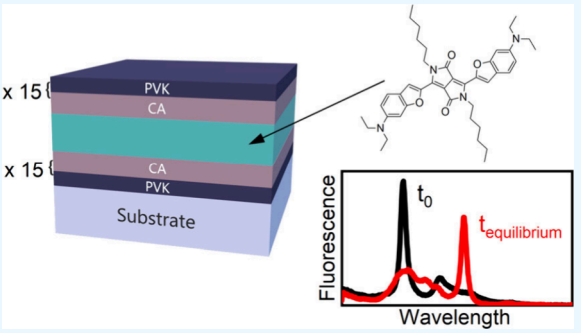

INTRODUCTION

The escalation in production and consumption of goods has been increasingly leading to a continuous discharge of harmful chemicals into the atmosphere. Among these pollutants, volatile organic compounds (VOCs) are of particular concern due to their impacts on the environment and on human health. Indeed, even seemingly innocuous solvents like acetone can induce neurological damage, while tetrachloroethylene, which is widely employed in dry cleaning processes, is a suspected carcinogen.[1] VOCs are released in the environment by many industrial processes such as oil refineries, power plants, and chemical manufacturing. In particular, urban sources include painting, dry cleaning, and refrigeration processes. Usually, quantitative monitoring makes use of highly sensitive yet unselective portable detectors like colorimetric tubes and infrared sensors;[2] on the contrary, qualitative assessment needs complex sampling procedures and laboratory analyses.[3] Therefore, developing simple systems to identify and monitor these compounds in both residential and occupational environments would be advantageous for safeguarding public health.

Within this context, colorimetric detection based on polymer planar photonic crystals, namely Distributed Bragg Reflectors (DBRs) or other bioinspired photonic nanostructures, offers selectivity without chemical functionalization and has already shown the ability to detect several families of compounds in the vapor phase.[1,4−14] The interest in these devices arise from their simple and scalable fabrication, that makes them highly desirable in the field of disposable transducers.[15,16] DBRs are periodic structures composed of alternating layers of materials with different refractive indexes. The spacing between the layers is designed to create coherent diffraction of impinging light. The layer spacing is engineered to produce coherent diffraction of incident light. This periodicity alters the nanostructure's spectrum and creates characteristic reflectance peaks known as photonic bandgaps (PBGs), that provide them with their distinctive intense color. The spectral position of the PBGs can be approximated by the Bragg-Snell law:[17]

$$\lambda_{PBG} = 2(d_L + d_H)\sqrt{\frac{d_L n_L^2 + d_H n_H^2}{d_L + d_H}}$$

where n_H and n_L are the refractive indexes of the high-index and low-index layers respectively, while d_H and d_L are their

Received: June 19, 2024
Revised: August 28, 2024
Accepted: September 3, 2024
Published: October 2, 2024

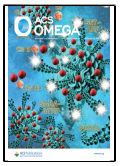

https://doi.org/10.1021/acsomega.4c05710
ACS Omega 2024, 9, 42375−42385

thicknesses. When used in sensing, DBRs harness the capability of polymers to adsorb volatile molecules. The analytes diffusivity, their sorption coefficient, and intercalation capability within polymers is mainly determined by the molar volume (V^M) of the analytes and the intermolecular interaction between the analytes and the polymer macromolecules. Such interactions can be predicted by the Hildebrand solubility parameter ($\Delta\delta^2$) for the polymer-analyte pairs. These parameters represent the difference of cohesive energy density between the two species[18] so that, the smaller the $\Delta\delta^2$, the larger the solubility and the analyte intercalation kinetics. The combination of both $\Delta\delta^2$ and V^M is summarized in the Flory–Huggins parameter $\left(\chi_{AP}^{H} = V^{M}\frac{\Delta\delta^2}{RT}\right)$ that represents the enthalpic interaction between the species involved.[19] For sake of simplicity, we neglect here the entropic contribution of such interaction. Therefore, χ_{AP}^{H} rules the analyte intercalation kinetic within the structure and the magnitude of the sensor response. Indeed, high polymer-analyte affinities typically cause the fast intercalation of molecules within the polymer, leading to considerable swelling of the polymer layers. In turn, this swelling increases the DBR optical pitch, and therefore shifts the PBG to longer wavelengts.[17] This shift is usually detected in the reflectance spectrum of the sensor. Thanks to the dependence of the intercalation kinetics and magnitude on χ_{AP}^{H}, the response to different analytes (including aromatic molecules, alcohols, chlorinated and fluorinated compounds) can be easily differentiated through careful selection of the polymers.[1,5−7,20] However, DBR sensors have an important drawback: the PBG signature used for detection is typically on the order of several tens of nanometers, which makes detecting small spectral variations a challenging task. To overcome this drawback, spectrally sharper features can be inserted within the PBG by introducing a defect in the lattice to break its periodicity. These sharp features are called defect modes,[21−23] and the whole structure takes the name of Planal microcavity. The defect layer, which consists of a film with different optical thickness than the other layers of the stack, can be doped with a fluorescent dye whose emission spectrum superimposed with the PBG and the defect mode. In this case, the dye emission is redistributed, resulting in a sharp and intense emission at the wavelengths corresponding to the defect mode, and a signal suppression at the PBG wavelengths. The defect mode of the microcavity, along with the resulting new emission feature of the dye, is sensitive to the structural variations of the DBR lattice, similarly to the PBG. However, the photoluminescence (PL) signal is much sharper than the latter, promising the capability to detect very small spectral variation. Microcavity sensors have already been developed; however, they are usually made of porous inorganics, like silicon, which require long and complex fabrication.[24−26] Some works study the fabrication of microcavity sensors by spin-coating,[27,28] while polymer-based microcavities are rare in literature.[29]

In this work, we incorporate a fluorescent diketopyrrolopyrrole (DPP) derivative in a spun-cast microcavity to allow analyte detection by both transmission and fluorescence probing. DPPs first uses date back to the early 1970s[30] when these molecules were commercialized as red pigments for high-end applications.[31−33] Indeed, they exhibit large molar absorption coefficient, large fluorescence quantum yield, and superior stability upon thermal stresses and irradiation.[34,35] All these elements are important to ensure that parasitic effects on the fluorescence signal can be avoided. This clearly demonstrates the role of the fluorescent microcavity as an effective transducer of the chemical signal into a physical one. Several researchers have reported on the use of DPPs as fluorescent probes,[36] as two-photon absorbing materials,[37] or in optoelectronic devices including organic field-effect transistors, organic light-emitting diodes, and organic photovoltaic cells.[38,39] Colorimetric and fluorescent sensors based on DPPs detect pH changes,[40] ions,[41] thiols,[42] and other compounds,[43−45] depending on the *C*-aryl and *N*-alkyl groups present.[36] While most of the literature on this topic focuses on solution sensing, a few papers have investigated DPPs as probes for vapor analytes when embedded in a solid matrix.[43−46] However, a solid matrix is desirable in sensing. Then, a solid DPP probe in the form of high optical quality thin films in combination with photonic nanostructures can become the two starting points to develop a sensor for detecting VOCs in the atmosphere.

In essence, to achieve the selectivity required to detect different VOCs species with a single photonic element, we combine a fluorescent probe consisting of a DPP derivative, and microcavity structure. The comprehensive response of the microcavity to the analytes leads to a dual probe system in which a single photonic element converts the chemical signal into optical ones. In this way, the response of the sensor is reflected in both the transmission (spectral shift of the PBG due to the swelling of the layer) and fluorescence (spectral shift, intensity changes driven by spectral redistribution and the interaction of electronic states between the analyte and DPP) signals. We target a proof-of-concept demonstration of a label-free sensor for VOCs, focusing foremost on selectivity. First, the fluorescence response of a polystyrene (PS) film with embedded DPP is evaluated to verify its characteristic response to four vapor analytes: toluene, 1-butanol (BuOH), acetone, and dichloromethane (DCM). Then, a microcavity is fabricated alternating layers of cellulose acetate (CA) and poly(*N*-vinylcarbazole) (PVK), casting a central PS layer with embedded DPP; the sensor is then tested with the same analytes.

RESULTS

Before performing the sensing measurements, we investigated the optical properties of DPP (whose structure is outlined in Figure 1a) both in solution and in a PS blend. The toluene solution exhibits a cyan shade, and when illuminated with violet light, it generates a strong pink fluorescence, as depicted in the digital photograph in Figure 1b. Such emission is maintained in solid state polymer films. Figure 1c shows the normalized absorption (black) and fluorescence (red) spectra of the PS/DPP. The sample absorption has two intense charge-transfer bands at 655 nm and at 600 nm, typical of DPP-based D−π−A−π−D chromophores.[47−49] The emission peaks at 677 nm, with a Stokes shift of 22 nm, and shows a shoulder at 740 nm. We also investigated the DPP stability under prolonged laser excitation to disentangle effects owing to irradiation and/or thermal effects from those induced by a possible interaction with the analytes in the sensor. The film was then exposed for 100 min to the same laser source used for the sensing experiments, while continuously monitoring its emission signal. The DPP emission was slightly affected by irradiation, and the fluorescence intensity increased by 12% during the test (Supporting Information Figure S1).

Once placed into the microcavity structure, the dye emission is strongly modified, due to the spectral redistribution of the

https://doi.org/10.1021/acsomega.4c05710
ACS Omega 2024, 9, 42375−42385

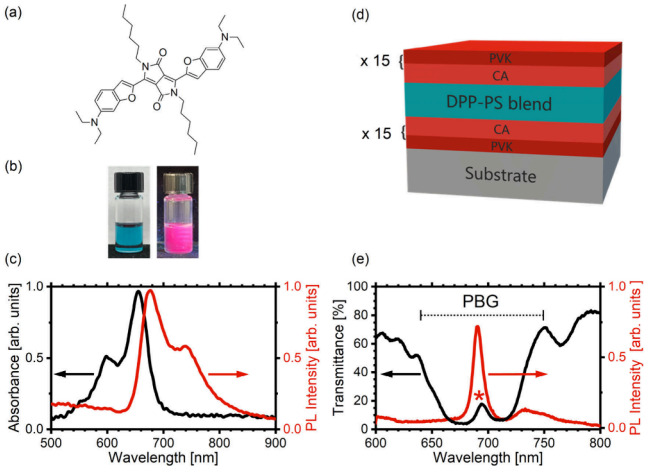

Figure 1. (a) Chemical structure of the DPP dye. (b) Photographs of a DPP solution in toluene under white light (left) and irradiated by 405 nm light source (right). (c) Normalized absorption (black line) and fluorescence spectra (red line) of the PS/DPP film. (d) Structure of the microcavity: each DBR is composed of 15 alternated bilayers of PVK and CA, while the central layer is the PS/DPP blend. (e) Transmission (black line) and fluorescence (red line) spectra of the microcavity. The cavity mode is marked with "*" while the PBG width is highlighted by the dotted line. All the fluorescence spectra have been excited at 405 nm. The microcavity has been grown on a glass substrate.

PL oscillator strength.[17] Figure 1d sketches the structure of the cavity, which is made of two PVK-CA multilayers enclosing a central defect layer made of PS/DPP. Figure 1e compares the transmission (black line) and the fluorescence spectra of the structure (red line). The transmission was measured at an incidence angle of 25° to enable simultaneous measurement of both the signals using the same setup. In these conditions, the PBG of the structure falls in between 640 and 750 nm (dotted line in the figure). In the center of the PBG, a sharp maximum in transmittance is assigned to the cavity mode, at 694 nm (marked with an asterisk). The structure heavily influences the DPP fluorescence, that now shows a sharp peak at 691 nm, which corresponds to the cavity mode, and a much weaker band at 733 nm, at the PBG edge. The reflectance (see Supporting Information Figure S2), angle-resolved transmission and PL (see Supporting Information Figure S3) spectra of the microcavity were also measured and report the typical angular dispersion expected for the structure, with both PBG and cavity mode shifting toward shorter wavelengths as the angle increases.[17] The maximum intensity in fluorescence is detected at 25° (Supporting Information Figure S3c).

Prior to the microcavity sensor tests, the PS/DPP films were exposed to the four investigated analytes to study the effect of the volatile molecules on the dye without the additional effect of the microcavity structure. Figure 2 shows the fluorescence (a, c, e, g) and absorbance (b, d, f, h) spectra of the PS/DPP films during exposure and at equilibrium to toluene (a, b), 1-butanol (c, d), acetone (e, f), and DCM (g, h). All analytes cause fluorescence quenching, but the response time varies depending on the analyte, with 1-butanol being the slowest. Toluene causes a slight blue shift of the main fluorescence peak by 10 nm with an initial 48% increase in intensity, followed by a decrease, until an equilibrium value is reached (Figure 2a). 1-Butanol and acetone cause an initial red shift of 10 nm, with a subsequent blue shift of 5 nm only in the case of butanol (Figure 2c and e). Again, the intensity of the main peak initially increases, albeit to a lesser extent. Dichloromethane exposure results in an initial red shift, followed by a blue shift of 3 nm, while the signal attenuates without an initial increase in emission intensity (Figure 2g). As for absorption, toluene and acetone cause significant changes in the shape of the spectrum (Figure 2b and f, respectively). In fact, as depicted in the digital photographs of the samples collected before and after exposure displayed as round inset in Figure 2b and f, the color of the film visibly changes. Moreover, such variation persists even after removal of the analyte from the sample atmosphere. In details, for toluene, the main peak at 655 nm and the shoulder at 600 nm are no longer visible, while two larger and less intense absorption signals are detected at 590 and 715 nm (Figure 2b). The weak spectral feature at 450 nm is red-shifted by 10 nm. When the exposed compound film is redissolved in toluene (Supporting Information Figure S4), there is no noticeable difference between pristine solved DPP and the redissolved one, indicating that there is no or minimal irreversible chemical change in the emitting molecule. Acetone shows a very similar effect, with two new broader absorption peaks at 570 and 700 nm (Figure 2f). In opposition, 1-butanol and dichloromethane do not alter the shape of the absorption but they reduce its intensity (Figure 2d,h).

Once this preliminary characterization was completed, we exposed the microcavities to the same four analytes. Table 1 reports the physicochemical properties of the compounds and of the polymer-analyte couples.[18,50] These parameters were indeed employed to design the structure. The Hildebrand solubility parameters δ_{tot} for the analytes and the polymers have been calculated from the relative Hansen parameters found in literature.[18] For each polymer-analyte pair, the difference $\Delta\delta$ and the Flory–Huggins parameters (χ) have been calculated. According to $\Delta\delta$ and χ values, 1-butanol is more soluble in CA,[20,51] while toluene, acetone, and dichloromethane appear to have a higher affinity to PVK and PS. We then expect a correspondent layer thickness increase upon vapor exposure.

Figure 3 shows the response of four sensors exposed each to one of the analytes. The transmission and fluorescence spectra during the exposure are reported as contour plots, with the exposure time on the y-axis, wavelength on the x-axis, and transmission or fluorescence intensity as the color scale. Supporting Information Figures S5, S6, S7, and S8 show the corresponding transmission and fluorescence spectra at selected exposure times.

In the case of toluene, the PBG of the sample is initially centered at 680 nm, and it is visible as a purple band in the contour plot reported in Figure 3a, with the cavity mode positioned at 675 nm (in blue shades). During the 4 h and 30 min exposure, the PBG shifts to 820 nm (140 nm shift). However, the shape of the spectrum changes drastically during the experiment. The PBG initially broadens; then, after 1 h and 30 min, two distinct transmission minima are present; they are visible in the contour as two purple bands divided by a relative maximum in yellow-green centered at 730 nm. The first minimum is approximately in the same spectral position as the initial PBG, while the second is at longer wavelengths. The two minima then red-shift by about 100 nm and begin to merge again; only after 3 h and 30 min a single PBG with a defined shape emerges again, centered at 800 nm (see also Supporting Information Figure S5). After another hour, the PBG reaches its equilibrium position. The initial fluorescence spectrum

https://doi.org/10.1021/acsomega.4c05710
ACS Omega 2024, 9, 42375−42385

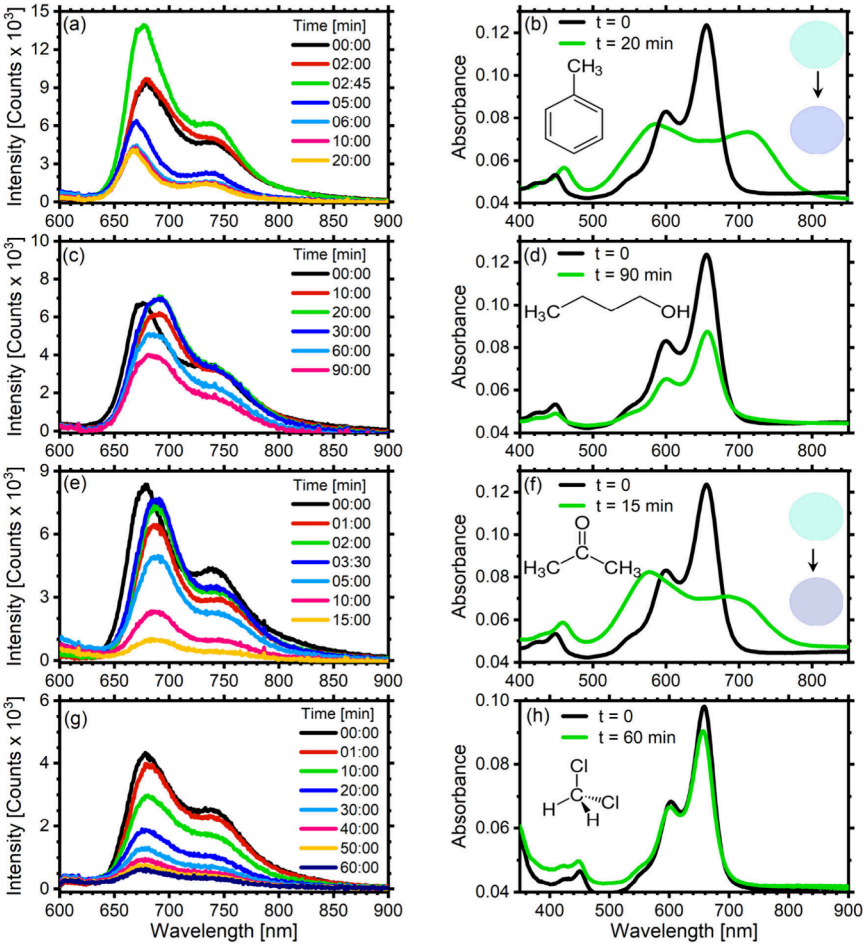

Figure 2. Fluorescence spectra of the PS/DPP film before exposure (black line) and at equilibrium (green line) for the four analytes: (a) toluene, (c) 1-butanol, (e) acetone, (g) dichloromethane. The corresponding absorbance for pristine PS/DPP film (black line) and exposed films (green line) to the analyte vapors are shown in (b) toluene, (d) 1-butanol, (f) acetone, (h) dichloromethane. The insets in (b) and (f) represent the color of the films before and after the exposure to toluene and acetone.

Table 1. Physicochemical Properties of the Analytes (Vapor Pressure, P_{vap}, and Molar Volume, V^M); Hildebrand Total Solubility Parameter (δ_{tot}) of the Analytes and the Polymers, Obtained from the Three Hansen Solubility Parameters;[18] Difference in the Hildebrand Solubility Parameter ($\Delta\delta^2$), Flory–Huggins Parameter (χ)

	P_{vap} (25 °C) [kPa][50]	V^M [Å^3][18]	δ_{tot} [MPa$^{1/2}$][18]	$\Delta\delta^2_{CA}$	χ_{CA}	$\Delta\delta^2_{PVK}$	χ_{PVK}	$\Delta\delta^2_{PS}$	χ_{PS}
Toluene	3.79	177.3	18.16	40.49	1.75	5.01	0.22	1.20	0.05
BuOH	0.89	151.9	23.20	1.77	0.07	7.81	0.29	15.51	0.57
Acetone	30.61	122.9	19.94	21.10	0.63	0.22	0.007	0.46	0.01
DCM	57.98	106.1	20.20	18.71	0.48	0.04	0.001	0.89	0.02
CA	-	-	24.53	-	-	-	-	-	-
PVK5	-	-	20.40	-	-	-	-	-	-
PS			19.26	-	-	-	-	-	-

(Supporting Information Figure 3b and Figure S5) is clearly affected by the presence of the cavity mode, which causes an intense emission peak at 675 nm (red in the contour) and two shoulders at 715 and 750 nm. The shape and intensity of the spectrum change during the exposure owing to the influence of the transmission spectrum, which changes dynamically (Figure 3b; the arrow shows the direction of the shift relative to the emission maximum). However, after 2 h and 15 min, the emission has almost completely disappeared due to the fluorescence quenching effect of toluene. Compared with the PS/DPP film exposed to toluene, the quenching effect is delayed in the case of the microcavity, because the toluene molecules must first permeate the first half of the microcavity to reach DPP. However, once the analyte front reaches the central defect, toluene causes stronger fluorescence quenching in the microcavity than in the case of the PS/DPP films.

When the microcavity is exposed to 1-butanol (Figure 3c,d and Supporting Information Figure S6), the response is much slower. In transmission, the PBG shifts by a total of 90 nm and reaches 770 nm at equilibrium. Again, the shape of the spectrum is not maintained throughout the exposure and after 30 min a second transmission minimum occurs; both bands, separated by a relative maximum, red-shift. After 4 h, the PBG at low wavelengths becomes less intense and merges with the main PBG at 770 nm. The fluorescence signal exhibits a complex behavior. The intensity of the main emission peak at

https://doi.org/10.1021/acsomega.4c05710
ACS Omega 2024, 9, 42375−42385

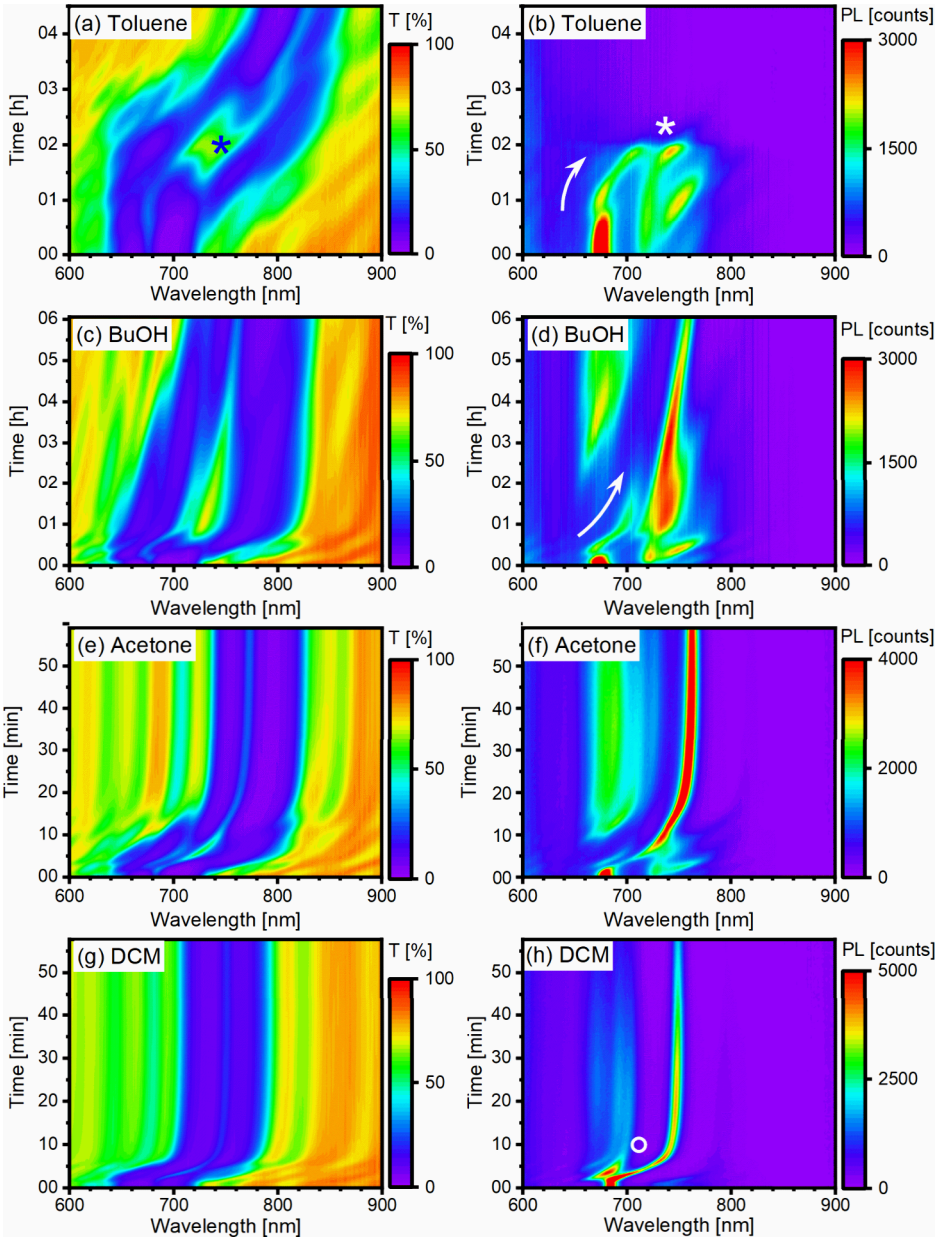

Figure 3. Optical response of the microcavity during exposure to the analytes: (a, c, e, g) transmittance and (b, d, f, h) fluorescence dynamic response. (a, b) Toluene; (c, d), 1-butanol; (e, f), acetone; (g, h) DCM. The arrows are guides-for-eyes to highlight the spectral shift while asterisk and open circle marks highlight significant points in the evolution of the fluorescence signal for toluene and DCM, respectively; additional details are provided in the text.

675 nm decreases by 60% after the first 15 min; then the peak red-shifts following the maximum in the transmission spectrum (Figure 3d; the arrow shows the direction of the shift). At the same time, new peaks appear at longer wavelengths, changing their intensity and spectral position during the exposure. After 1 h, the peak at 730 nm becomes sharper and shifts along with the transmission maximum until the equilibrium position is reached. The emission also increases again in the region to the left of the PBG, between 650 and 675 nm. However, the fluorescence signal at equilibrium is reduced due to the quenching effect of the analyte.

The microcavities exposed to acetone and dichloromethane show a different behavior than those exposed to toluene and 1-butanol. Indeed, the response is faster, resulting in less drastic changes in the shape of the PBG in transmission and in the presence of a definite emission peak in fluorescence. In the case of acetone (Supporting Information Figure 3e and Figure S7), the PBG shifts by 100 nm from 685 to 775 nm in only 30 min. The shape of the PBG and the cavity mode are not always maintained during the experiment: between 3 and 15 min, the PBG broadens and then splits into two minima, but after 20 min the original shape is restored. In fluorescence, the main peak in the contour plot of Figure 3f appears to shift to longer wavelengths, from 680 to 762 nm following the transmission maximum. At 12 min after the beginning of the exposure, the emission intensity increases in the range between 650 and 720 nm. This signal is visible in the contour plot as a green band. When equilibrium is reached the intensity of the main peak (now at 762 nm) has decreased by 40% compared to the initial value (Supporting Information Figure S7).

https://doi.org/10.1021/acsomega.4c05710
ACS Omega 2024, 9, 42375−42385

When the microcavity is exposed to dichloromethane (Supporting Information Figure 3g and Figure S8), the response is even faster, with a 60 nm shift in transmittance in the first 10 min. The shape of the PBG and the cavity mode are preserved during the red shift from 680 to 750 nm (a shift of 70 nm), except for a broadening of the PBG between 2 and 4 min after the start. The main peak of the fluorescence signal shifts from 684 to 749 nm following the cavity mode; during the first 2 min, its intensity increases, but when equilibrium is reached, the intensity is 25% of the initial value (Supporting Information Figure S8). During the exposure, a second emission peak appears between 669 and 700 nm, leading to a second red spot in the contour plot (highlighted by an asterisk in Figure 3h) next to the red line corresponding to the main peak. This second peak appears quickly, but then its intensity decreases, leaving only a cyan band in the contour. Gradually, the two emission peaks shift apart until, after 6 min, the peak at shorter wavelengths is at the left edge of the PBG (Supporting Information Figure S9). Table 2 provides a comprehensive summary of the spectral changes observed in transmittance and fluorescence when the microcavity is exposed to the analytes, as described in the following paragraphs.

Table 2. Summary of the Transmittance and PL Spectral Changes That Occur When the Microcavity Is Exposed to the Analytes[a]

	$\lambda_{i\text{-}PBG}$ [nm]	$\lambda_{f\text{-}PBG}$ [nm]	$\Delta\lambda_{PBG}$ [nm]	$\lambda_{i\text{-}PL}$ [nm]	$\lambda_{f\text{-}PL}$ [nm]	$\Delta\lambda_{-PL}$ [nm]
Toluene	680	820	140	675	-	-
BuOH	680	770	90	675	760	85
Acetone	685	775	100	680	762	82
DCM	680	750	70	684	749	65

[a] $\lambda_{i\text{-}PBG}/\lambda_{i\text{-}PL}$ = initial PBG minimum/PL maximum wavelength: $\lambda_{f\text{-}PBG}/\lambda_{f\text{-}PL}$ = final equilibrium PBG minimum/PL maximum wavelength; $\Delta\lambda_{PBG}/\Delta\lambda_{-PL}$ = spectral shift between initial and final PBG minimum/PL maximum wavelength.

DISCUSSION

When the DPP/PS film is exposed to the analytes, the shift of the fluorescence and absorbance spectra suggests a change in the energy levels of the dye molecules, especially in the case of exposure to toluene and acetone (Figure 2). The quenching mechanism is unknown, because there are no quenching studies on this specific DPP derivative, either in solution or in a matrix. However, when the film is redissolved in toluene after exposure to the analyte vapors, the original absorption spectrum of the solution is restored (Supporting Information Figure S4), indicating that no irreversible reactions between the analytes and DPP have occurred, and that the origin of the effect is physical. The DPP derivative used in this work exhibits solvatochromism in solution,[47] but when the dye is embedded in a polymer, its environment is modified by the interactions that can take place between the dye, the polymer, and the analyte molecules that permeate the matrix. A simple solvatochromic effect is not sufficient to explain the observed emission shifts. The properties of some other DPP derivatives in the solid state have been investigated.[52−57] However, there are very few studies in the literature on the effects of solvent vapors on DPPs in the solid state[58−61] or on DPPs embedded in polymer matrices.[43,44] Mizuguchi et al. studied three DPP derivatives (with different chemical groups) in the solid state exposed to acetone vapors.[58] The vapors lead to crystallization and to changes in the absorption spectra analogous to those presented here, with a new peak forming at higher wavelengths with respect to its initial emission spectrum. This may suggest that changes in our PS/DPP films are related to a rearrangement of the DPP molecules within the polymer

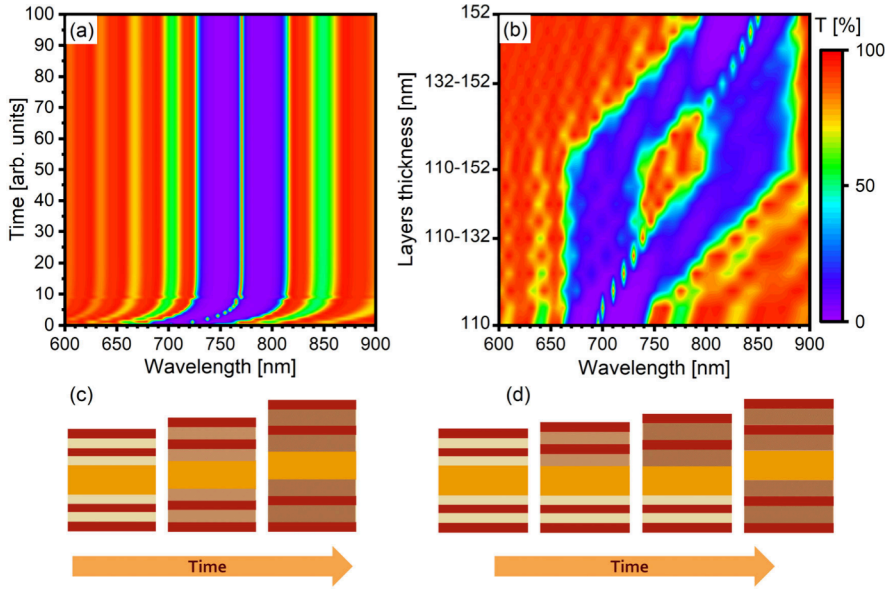

Figure 4. (a) Simulated transmittance contour plot assuming that all the sensitive layers and the microcavity swell simultaneously. (b) Simulated transmittance contour plot, with gradual swelling of the layers of the microcavity. (c, d) Schematic of the swelling process: The different colors represent PVK (red), CA (light yellow), and the microcavity layer (orange). The swelling of the CA is indicated by a color shift from light yellow to brown. In detail: (c) swelling scheme for simultaneous swelling of the layers when only one of the two polymers swells in response to analyte intercalation; (d) gradual swelling scheme, assuming the superior half of the microcavity swells first. Red layer, PVK film; yellow layer, CA film; orange layer, DPP:PS film.

https://doi.org/10.1021/acsomega.4c05710
ACS Omega 2024, 9, 42375−42385

matrix. The matrix itself could have an influence; when an emitter is embedded in a polymer matrix, the effectiveness of a solvent vapor treatment generally depends on the affinity of the solvent for the fluorophore, but also for the polymer, since the solvent can affect the mobility of the polymer chains and facilitate migration of the dye.[62−64] Therefore, our hypothesis is that when the analyte molecules enter the PS matrix, they act as plasticizers and facilitate the migration of the DPP molecules, which then form aggregates, leading to fluorescence quenching and changes in absorbance.

Exposure of the microcavities to the four analytes showed that a significant response can be obtained for both transmission and fluorescence. The changes in transmission are, in fact, the main cause of the changes in the fluorescence spectra: in all cases, emission is suppressed when the PBG minimum overlaps with the dye emission wavelengths, and it is enhanced when the cavity mode falls in the same spectral range (Figure 3). Indeed, the main emission peak red-shifts when the cavity mode shifts. The analytes also directly affect the DPP by quenching its fluorescence, but this effect becomes relevant only after the analyte molecules have permeated at least half of the microcavity structure, i.e., after the analyte has reached the PS/DPP defect layer. This is particularly evident in the case of toluene, where a drastic fluorescence quenching effect occurs while there are two minima in the corresponding transmission spectra (this point has been highlighted with an asterisk in Figure 3a.b). The presence of two minima indicates that there are two sections of the microcavity with different periodicities. This means that the toluene molecules must diffuse layer by layer in the sample, so that at some point one section of the microcavity is swollen and gives the transmission minimum at longer wavelengths, while the second section of the microcavity is still unaffected by toluene and gives a minimum at the original spectral position of the PBG. This is also consistent with the hypothesis that a compact analyte front causes a strong and sudden emission quenching when it reaches the defect. In contrast, when the microcavity is exposed to acetone and dichloromethane, the PBG shifts while maintaining its shape. This effect is possible if the analyte molecules diffuse very rapidly through the multilayer, so that the polymer layers swell all together and the layer thicknesses are always homogeneous throughout the stack.

To provide an interpretation for the response of the sensors qualitatively, we calculated the transmittance spectra in a simulation of the two opposite cases of polymer swelling. The details of the procedure are described in the Experimental Section. The progressive change of layer thickness is modeled in the simulations, while the initial starting value was determined by atomic force microscopy (AFM; Supporting Information Figure S9). In the first simulation, all layers of one of the polymers are assumed to swell simultaneously (Figure 4a and scheme in Figure 4c); the periodicity of the structure is maintained and a definite PBG is present in the spectra at all times. In the second simulation, gradual swelling is assumed (Figure 4b,d). In this case, the PBG in the contour plot of the simulation (Figure 4b) splits into two transmission minima as the asymmetry of the structure increases; the first minimum is at the same wavelengths as the original PBG, and the second minimum is at longer wavelengths. Comparison of the simulation with the experimental results shows that systems exposed to dichloromethane fall into the first category; systems exposed to toluene or 1-butanol fall into the second category, while exposure to acetone is an intermediate case, since there is a time interval between 3 and 15 min in which the PBG loses its shape.

Ultimately, the distinct response of the microcavity sensor to the analytes is evident even when considering a single fluorescence spectrum, rather than relying on the entire time response shown in contour plots. Indeed, after 30 min of exposure to the vapors, the shape of the fluorescence spectra is markedly different in the four cases (Figure 5). In addition, the response time can be easily tuned by modifying the microcavity structure[1] to reach responses as short as few minutes[5,65] or less.[66]

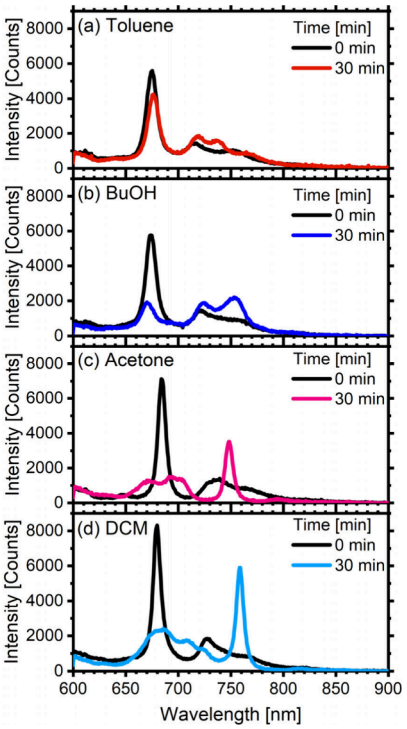

Figure 5. Microcavity fluorescence spectra before (black line) and after (colored lines) 30 min of exposure to (a) toluene, (b) 1-butanol, (c) acetone, and (d) DCM.

Addressing the fundamental physical mechanisms governing the observed changes in fluorescence is rather complex. While the response detected in transmittance is related to the swelling of the microcavity and can be predicted through proper modeling, the fluorescence is affected by variations in both the electronic structure of DPP and the dielectric environment. Figure 2 suggests that the PL changes can be attributed to a quenching mechanism, along with a second process that also affects the absorbance spectrum of the molecule. We propose that this behavior is associated with a physical aggregation effect on DPP. Additionally, the swelling of the microcavity layers generates a dynamic spectral redistribution of the PL signal and can induce variations in its radiative rate.[21,22] While spectral redistribution is highly significant for analyte detection, changes in radiative rate are of low significance for this purpose and beyond the scope of this paper.

In summary, the microcavity has proven to be a promising sensor for the selective detection of organic molecules in the vapor phase. The selectivity of the sensor results both from the different affinity of the analytes for CA, PVK and PS, and from

https://doi.org/10.1021/acsomega.4c05710
ACS Omega 2024, 9, 42375−42385

the effect of each analyte on the DPP fluorophore, which in some cases leads to aggregation. Such a sensor—perhaps integrated in a chip[67,68] - could find application in many fields where optical probes based on polymeric photonic crystals can be used as VOC sensors, from environmental monitoring to the industrial sector (e.g., for indoor pollution detection and food spoilage detection)[4,69] and even for biomedical applications.[4,69] This approach has also been reported for the discrimination of different analytes employing chemometric approaches.[20] In this sense, utilizing both PL and transmittance to probe the response adds an additional variable, enhancing the potential of these sensors for qualitative assessment in complex mixtures.

CONCLUSIONS

A polymer planar microcavity with an embedded fluorescent diketopyrrolopyrrole derivative was developed as a sensor for the detection of volatile organic compounds. Four solvents with different polarity and molecular volume have been tested. The diketopyrrolopyrrole dye was found to be sensitive to the analyte vapors by fluorescence quenching even when not embedded in a microcavity. Aggregation effects are observed upon exposure to toluene and acetone. However, the microcavity offers several advantages over a sensor based solely on the emission of the dye. The microcavity sensor can detect and identify analytes based on two different mechanisms, namely the time evolution of the transmission spectrum of the microcavity and the corresponding modification of the fluorescence signal of the dye. When the microcavity sensor is exposed to the vapors, the transmission changes affect the shape and intensity of the fluorescence spectrum, making it easier to detect the changes caused by exposure to the analytes. In addition, the narrow emission peak due to the spectral redistribution of the dye fluorescence operated by the cavity mode facilitates the identification and detection of the analyte. The highlighted selectivity of the microcavity sensor is due to the characteristic interaction of the analytes with both the polymers of the photonic crystals and with the diketopyrrolopyrrole dye. The microcavity offers the possibility of detecting the analytes in two different ways, i.e. by considering the entire time response or by selecting appropriate individual spectra. The significant variation in spectra depending on the analyte shows promise for identifying different classes of molecules using the same sensor, without the need for specific receptors.

EXPERIMENTAL SECTION

Microcavity Fabrication. The microcavities were fabricated by spin-coating on a glass substrate, alternating layers of poly(*N*-vinylcarbazole) (PVK, Acros Organic, M_w = 135600 g/mol, M_n = 56400 g/mol; refractive index n = 1.692 at 550 nm)[70] and cellulose acetate (CA, Sigma-Aldrich, M_n = 50000 g/mol; n = 1.477 at 550 nm),[71] as the high and low refractive index materials respectively on a microscope glass substrate. The dielectric contrast between the two polymers is Δn = 0.215 at 550 nm. For the process, 33 mg/mL of CA were dissolved in 4-hydroxy-4-methylpentan-2-one (Sigma-Aldrich, 99%), while PVK was dissolved in toluene (ACS Reagent, >99.5%), with a concentration of 35 mg/mL. Both solutions (100 μL) were spin-cast at 170 rps on glass substrates. Each of the two DBR mirrors composing the cavity consists of 30 alternated CA and PVK layers. Every four layers, the samples were thermally annealed at 75 °C, for 1 min on a hot plate. The defect layer in between the two DBRs was obtained casting at 50 rps a toluene solution (150 μL) containing 2,5-dihexyl-1,4-diketo-3,6-di(6-(diethylamino)-2-benzofuryl)-pyrrolo[3,4-*c*]pyrrole (DPP, concentration 1 mg/mL, Supporting Information Figure S10) and polystyrene (PS, concentration 30 mg/mL; Sigma-Aldrich, M_w = 192000 g/mol, refractive index n= 1.593 at 550 nm).[70,72] Identical procedure was employed to cast the DPP reference thin film on glass substrates. The DPP was synthesized following the literature procedure by Koszarna et al.[47]

Optical Characterizations. Absorbance spectra were collected for both DPP film and solution with a UV—vis spectrometer (Shimadzu UV-1800, 1 nm resolution). Photoluminescence spectra were instead collected upon excitation with a CW 448 nm, 40 mW laser (Changchun New Industries Optoelectronic Tech) and collected with an Avaspec-ULS2048CL-EVO-RS detector (spectral range 200—1100 nm, resolution 1.4 nm) in an optical fiber optical setup.

Reflectance spectra were measured with a Y-probe optical fiber probe (FCR-7UVIR200, Avantes). The light source was a deuterium-halogen lamp (DH-2000-BAL, Ocean Optics, spectral range 230—2500 nm). The reflected signal collected with an Avaspec-ULS2048CL-EVO-RS detector (spectral range 200—1100 nm, resolution 1.4 nm). An aluminum mirror was used for the white reference spectrum. Angle-resolved transmission was measured with a homemade optical setup comprising optical fibers (FG400AEA, diameter 400 μm, NA 0.22), coupled with the deuterium-halogen lamp (DH-2000-BAL), and with the spectrometer (Avaspec-ULS2048CL-EVO-RS); the spectra are measured every 5°, going from 0° to 70°. Angle-resolved fluorescence is measured with a similar setup, but the sample is irradiated with a continuous laser source, previously described.

Sensing Measurements. For each analyte, a PS/DPP or microcavity sample was placed in a quartz cuvette closed with a bulb containing a liquid reserve of the analyte to saturate the environment. The selected analytes were toluene (ACS Reagent, >99.5%), 1-butanol (Sigma-Aldrich, 99.9%), acetone (Sigma-Aldrich, Chromasolv, >99.8%), and dichloromethane (Supelco SupraSolv, >99.8%). The calculated vapor concentrations (25 °C) are 0.141 mg/L, 0.026 mg/L, 0.394 mg/L 1.131 mg/L respectively. During exposure, the transmission (absorbance for PS/DPP film) and fluorescence of the microcavity were measured on the same spot of the sample, set time intervals. Transmittance/absorbance was collected with a fiber-based setup consisting of the light source previously mentioned and a CCD spectrometer (AvaSpec-ULS2048XL, spectral range 200—1150 nm, 1.4 nm resolution) at 0° from the normal direction to the surface of the microcavity. Simultaneously, PL measurements were performed exciting the sample with the 448 nm laser and detecting the signal with the Avaspec-ULS2048CL-EVO-RS. An automatic shutter blocked the laser beam in between the measurements to prevent constant irradiation of the dye. For practical, geometrical reasons, there is an angle of 25° degrees between the fluorescence collection system and the normal direction to the surface of the sample. Because of this, in the case of the spectra measured during the exposure to the analytes, the transmission spectrum has been rigidly blue-shifted by 20 nm as discussed in the Results section.

Spectral Modeling. Response spectra were modeled with a MATLAB code based on the transfer matrix method, as

https://doi.org/10.1021/acsomega.4c05710
ACS Omega 2024, 9, 42375—42385

described in previous works.[22,23] The code considers the refractive index dispersions of the polymers and gives the simulated transmission spectrum of a microcavity, given the layer thicknesses. In the case of simultaneous swelling, the experiment with exposure to dichloromethane was used as a reference for the simulation. Layer thicknesses were fitted from the experimental spectra collected at the begin and at the end of the exposure. Subsequently, the film thicknesses were systematically varied in the simulations, to reproduce the changes in the transmission spectra due to the progressive swelling of the polymers over time. It is assumed that only one between CA and PVK swells when the analyte intercalates the structure, depending on which polymer has the greatest affinity for the analyte (smaller $\Delta\delta^2$). The layers of the other polymer act as a barrier to the penetration of the analyte molecules into the deeper layers. This assumption is based on previous works on DBR sensors.[51] In the case of dichloromethane, considering the Hildebrand and Flory–Huggins parameters listed in Table 1, the PVK layers and the PS defect layer are swelled. Based on previous works,[51] all layers are assumed to swell with time according to an exponential law ($d = a - b \cdot c^{-t}$), where d is the layer thickness and the parameters a, b, and c are different depending on the analyte and on the polymer considered (PVK or PS), in order to have initial and equilibrium thicknesses corresponding to those obtained by modeling the experimental spectra. The time scale is arbitrary; the thicknesses vary from the initial value at time 0 and reach the equilibrium value at time 100. In the case of gradual swelling, exposure to toluene is used as a reference for the initial and equilibrium spectral positions of the PBG. Again, the PVK is swollen when toluene intercalates the structure. Initially, only the first half of the microcavity is swollen, then the second half starts to swell as well. The film thicknesses are systematically varied in 5 nm steps from the initial to the final values.

Thickness Measurement. Atomic force microscopy (AFM) was used measure the thickness of the defect layer in tapping mode using a Nanosurf Core AFM microscope. Thickness was determined from the profile of a cross-section cut into the sample film. Two samples were prepared, the first was a CA film that served as a reference, and the second was a bilayer, with a PS/DPP layer on top of a CA layer. PS/DPP was cast using the same experimental parameters as the defect layer in the microcavities. The thickness of the reference layer was then subtracted from the total thickness of the bilayer. The scans were analyzed using the open-source software Gwyddion.[73] The measurement was repeated 5 times.

■ ASSOCIATED CONTENT

Supporting Information

The Supporting Information is available free of charge at https://pubs.acs.org/doi/10.1021/acsomega.4c05710.

Optical characterization of the PS/DPP film and of the microcavity; absorption spectrum of the PS/DPP before and after toluene exposure; transmission and fluorescence spectra of the microcavities during exposure to the analytes; AFM thickness measurements for a DPP/PS film; ^{1}H and ^{13}C NMR spectra of DPP (PDF)

■ AUTHOR INFORMATION

Corresponding Author

Davide Comoretto − *Dipartimento di Chimica e Chimica Industriale, Università di Genova, 16146 Genova, Italy;* orcid.org/0000-0002-2168-2851; Email: davide.comoretto@unige.it

Authors

Laura Magnasco − *Dipartimento di Chimica e Chimica Industriale, Università di Genova, 16146 Genova, Italy;* Present Address: RINA Consulting S.p.A., Via Antonio Cecchi 6, 16129 Genova, Italy

Andrea Lanfranchi − *Dipartimento di Chimica e Chimica Industriale, Università di Genova, 16146 Genova, Italy;* orcid.org/0000-0003-3642-2611

Martina Martusciello − *Dipartimento di Chimica e Chimica Industriale, Università di Genova, 16146 Genova, Italy*

Heba Megahd − *Dipartimento di Chimica e Chimica Industriale, Università di Genova, 16146 Genova, Italy;* Present Address: ASML Netherlands B.V., De Run 6503m 5504 DR Veldhoven, The Netherlands; orcid.org/0000-0003-2385-6648

Giovanni Manfredi − *Novavido S.r.l., 40133 Bologna, Italy;* orcid.org/0000-0003-0682-0731

Paola Lova − *Dipartimento di Chimica e Chimica Industriale, Università di Genova, 16146 Genova, Italy;* orcid.org/0000-0002-5634-6321

Beata Koszarna − *Institute of Organic Chemistry of the Polish Academy of Sciences, 01-224 Warsaw, Poland;* orcid.org/0000-0003-4716-7169

Daniel T. Gryko − *Institute of Organic Chemistry of the Polish Academy of Sciences, 01-224 Warsaw, Poland*

Complete contact information is available at: https://pubs.acs.org/10.1021/acsomega.4c05710

Author Contributions

The manuscript was written through contributions of all authors. All authors have given approval to the final version of the manuscript.

Notes

The authors declare no competing financial interest.

■ ACKNOWLEDGMENTS

Work in Genova was Funded by the European Union—NextGenerationEU and by the Ministry of University and Research (MUR), National Recovery and Resilience Plan (NRRP), Mission 4, Component 2, Investment 1.5, Project "RAISE—Robotics and AI for Socio-economic Empowerment" (Grant ECS00000035) as well as by PRIN 2020 Research Project "PETALS" (Grant 2020TS9LXS).

■ ABBREVIATIONS

VOCs, volatile organic compounds; DBR, distributed Bragg reflector; PBG, photonic bandgap; DPP, diketopyrrolopyrrole; PL, fluorescence; PVK, poly(*N*-vinylcarbazole); CA, cellulose acetate; PS, polystyrene; BuOH, 1-butanol; DCM, dichloromethane; AFM, atomic force microscopy; NA, numerical aperture; CCD, charge-coupled device

https://doi.org/10.1021/acsomega.4c05710
ACS Omega 2024, 9, 42375−42385

REFERENCES

(1) Megahd, H.; Lova, P.; Comoretto, D. Universal Design Rules for Flory-Huggins Polymer Photonic Vapor Sensors. *Adv. Funct. Mater.* **2021**, *31* (9), 2009626.

(2) Wong, J. Y.; Anderson, R. L. *Non-Dispersive Infrared Gas Measurement*; International Frequency Sensor Association Publishing: Barcelona, 2012.

(3) Pavia, D. L. *Introduction to Organic Laboratory Techniques: A Small Scale Approach.*, 2nd ed.; Thomson Brooks/Cole: Belmont, CA, USA, 2005; Vol. *1*.

(4) Serpe, M. J.; Kang, Y.; Zhang, Q. *Photonic Materials for Sensing, Biosensing and Display Devices*; Springer, 2016.

(5) Megahd, H.; Oldani, C.; Radice, S.; Lanfranchi, A.; Patrini, M.; Lova, P.; Comoretto, D. Aquivion-Poly(N-vinylcarbazole) Holistic Flory-Huggins Photonic Vapor Sensors. *Adv. Opt. Mater.* **2021**, *9* (5), 2002006.

(6) Escher, A.; Magnasco, L.; Martorelli, F.; Megahd, H.; Van Büren, B.; Dodero, A.; Steiner, U.; Comoretto, D.; Lova, P. From Landfill to Photonics: The Upcycling of Plastic Waste. *ACS Appl. Polym. Mater.* **2024**, *6* (12), 6917−6925.

(7) Lova, P.; Megahd, H.; Comoretto, D. Thin Polymer Films: Simple Optical Determination of Molecular Diffusion Coefficients. *ACS Appl. Polym. Mater.* **2020**, *2* (2), 563−568.

(8) Shen, N.; Hu, M.; Wang, X.-Q.; Sun, P.-Z.; Yuan, C.-L.; Liu, B.; Shen, D.; Zheng, Z.-G.; Li, Q. Cholesteric Soft Matter Molded Helical Photonic Architecture toward Volatility Monitoring of Organic Solvent. *Adv. Photonics Res.* **2021**, *2* (8), 2100018.

(9) Yang, Y.; Wang, L.; Yang, H.; Li, Q. 3D Chiral Photonic Nanostructures Based on Blue-Phase Liquid Crystals. *Small Science* **2021**, *1* (6), 2100007.

(10) Jeon, J.; Bukharina, D.; Kim, M.; Kang, S.; Kim, J.; Zhang, Y.; Tsukruk, V. Tunable and Responsive Photonic Bio-Inspired Materials and Their Applications. *Resp. Mater.* **2024**, *2* (1), No. e20230032.

(11) Zhang, Y.; Zheng, Z.-G.; Li, Q. Multiple Degrees-Of-Freedom Programmable Soft-Matter-Photonics: Configuration, Manipulation, and Advaced Applications. *Resp. Mater.* **2024**, *2* (1), No. e20230029.

(12) Foelen, Y.; Schenning, A. P. H. J. Optical Indicators Based on Structural Colored Polymers. *Adv. Sci.* **2022**, *9* (14), 2200399.

(13) Gao, L.; Kou, D.; Lin, R.; Ma, W.; Zhang, S. Ultrathin Photonic Crystal Based on Photo-Crosslinked Polymer and Metal-Organic Framework for Highly Sensitive Detection and Discrimination of Benzene Series Vapors. *J. Colloid Interface Sci.* **2024**, *666*, 572−584.

(14) Wei, J.; Yi, Z.; Yang, L.; Zhang, L.; Yang, J.; Qin, M.; Cao, S. Photonic Crystal Gas Sensors Based on Metal-Organic Frameworks and Polymers. *Anal. Methods* **2024**, *16*, 4901.

(15) Mao, G.; Andrews, J.; Crescimanno, M.; Singer, K. D.; Baer, E.; Hiltner, A.; Song, H.; Shakya, B. Co-extruded mechanically tunable multilayer elastomer laser. *Optical Materials Express* **2011**, *1* (1), 108−114.

(16) Singer, K. D.; Kazmierczak, T.; Lott, J.; Song, H.; Wu, Y.; Andrews, J.; Baer, E.; Hiltner, A.; Weder, C. Melt-processed all-polymer distributed Bragg reflector laser. *Opt. Express* **2008**, *16* (14), 10358−10363.

(17) Lova, P.; Manfredi, G.; Comoretto, D. Advances in Functional Solution Processed Planar 1D Photonic Crystals. *Adv. Opt. Mater.* **2018**, *6* (24), 1800730.

(18) Hansen, C. M. *Hansen Solubility Parameters: A User's Handbook*; CRC Press, 2007.

(19) Flory, P. J. *Principles of Polymer Chemistry*; Cornell University Press, 1953.

(20) Lova, P.; Manfredi, G.; Bastianini, C.; Mennucci, C.; Buatier de Mongeot, F.; Servida, A.; Comoretto, D. Flory-Huggins Photonic Sensors for the Optical Assessment of Molecular Diffusion Coefficients in Polymers. *ACS Appl. Mater. Interfaces* **2019**, *11* (18), 16872−16880.

(21) Megahd, H.; Villarreal Brito, M.; Lanfranchi, A.; Stagnaro, P.; Lova, P.; Comoretto, D. Control of Near-Infrared Dye Fluorescence Lifetime in All-Polymer Microcavities. *Mater. Chem. Front.* **2022**, *6*, 2413−2421.

(22) Megahd, H.; Lova, P.; Sardar, S.; D'Andrea, C.; Lanfranchi, A.; Koszarna, B.; Patrini, M.; Gryko, D. T.; Comoretto, D. All-Polymer Microcavities for the Fluorescence Radiative Rate Modification of a Diketopyrrolopyrrole Derivative. *ACS Omega* **2022**, *7* (18), 15499−15506.

(23) Kavokin, A.; Baumberg, J. J.; Malpuech, G.; Laussy, F. P. *Microcavities*; Oxford University Press: Oxford, 2017.

(24) Tokranova, N. A.; Novak, S. W.; Castracane, J.; Levitsky, I. A. Deep Infiltration of Emissive Polymers into Mesoporous Silicon Microcavities: Nanoscale Confinement and Advanced Vapor Sensing. *J. Phys. Chem. C* **2013**, *117* (44), 22667−22676.

(25) Martin, M.; Taleb Bendiab, C.; Massif, L.; Palestino, G.; Agarwal, V.; Cuisinier, F.; Gergely, C. Matrix Metalloproteinase Sensing via Porous Silicon Microcavity Devices Functionalized With Human Antibodies. *Phys. Status Solidi C* **2011**, *8* (6), 1888−1892.

(26) De Stefano, L.; Rendina, I.; Moretti, L.; Tundo, S.; Rossi, A. M. Smart Optical Sensors for Chemical Substances Based on Porous Silicon Technology. *Appl. Opt.* **2004**, *43* (1), 167−172.

(27) Szendrei, K.; Jiménez-Solano, A.; Lozano, G.; Lotsch, B. V.; Míguez, H. Fluorescent Humidity Sensors Based on Photonic Resonators. *Adv. Opt. Mater.* **2017**, *5* (23), 1700663.

(28) Sanchez-Sobrado, O.; Calvo, M. E.; Nunez, N.; Ocana, M.; Lozano, G.; Miguez, H. Environmentally Responsive Nanoparticle-Based Luminescent Optical Resonators. *Nanoscale* **2010**, *2* (6), 936−941.

(29) Clevenson, H.; Desjardins, P.; Gan, X.; Englund, D. High Sensitivity Gas Sensor Based on High-Q Suspended Polymer Photonic Crystal Nanocavity. *Appl. Phys. Lett.* **2014**, *104* (24), 241108.

(30) Farnum, D. G.; Mehta, G.; Moore, G. G. I.; Siegal, F. P. Attempted Reformatskii Reaction of Benzonitrile, 1,4-Diketo-3,6-Diphenylpyrrolo[3,4-C]Pyrrole. A Lactam Analogue of Pentalene. *Tetrahedron Lett.* **1974**, *15* (29), 2549−2552.

(31) Grzybowski, M.; Gryko, D. T. Diketopyrrolopyrroles: Synthesis, Reactivity, and Optical Properties. *Adv. Opt. Mater.* **2015**, *3* (3), 280−320.

(32) Bao, W. W.; Li, R.; Dai, Z. C.; Tang, J.; Shi, X.; Geng, J. T.; Deng, Z. F.; Hua, J. Diketopyrrolopyrrole (DPP)-Based Materials and Its Applications: A Review. *Front. Chem.* **2020**, *8*, 679.

(33) Rochat, A. C.; Cassar, L.; Iqbal, A. Preparation of pyrrolo-(3,4-c) pyrroles. EP0094911A3, 1983.

(34) Skonieczny, K.; Papadopoulos, I.; Thiel, D.; Gutkowski, K.; Haines, P.; McCosker, P. M.; Laurent, A. D.; Keller, P. A.; Clark, T.; Jacquemin, D.; Guldi, D. M.; Gryko, D. T. How to Make Nitroaromatic Compounds Glow: Next-Generation Large X-Shaped, Centrosymmetric Diketopyrrolopyrroles. *Angew. Chem.* **2020**, *59* (37), 16104−16113.

(35) Gutkowski, K.; Azarias, C.; Banasiewicz, M.; Kozankiewicz, B.; Jacquemin, D.; Gryko, D. T. Synthesis and Photophysical Properties of N-Arylated Diketopyrrolopyrroles. *Eur. J. Org. Chem.* **2018**, *2018* (47), 6643−6648.

(36) Kaur, M.; Choi, D. H. Diketopyrrolopyrrole: Brilliant Red Pigment Dye-Based Fluorescent Probes and Their Applications. *Chem. Soc. Rev.* **2015**, *44* (1), 58−77.

(37) Purc, A.; Koszarna, B.; Iachina, I.; Friese, D. H.; Tasior, M.; Sobczyk, K.; Pędziński, T.; Brewer, J.; Gryko, D. T. The Impact of Interplay Between Electronic and Steric Effects on the Synthesis and the Linear and Non-linear Optical Properties of Diketopyrrolopyrrole Bearing Benzofuran Moieties. *Org. Chem. Front.* **2017**, *4* (5), 724−736.

(38) Zhao, C.; Guo, Y.; Zhang, Y.; Yan, N.; You, S.; Li, W. Diketopyrrolopyrrole-Based Conjugated Materials for Non-fullerene Organic Solar Cells. *J. Mater. Chem. A* **2019**, *7* (17), 10174−10199.

(39) Jin, R.; Zhang, X.; Xiao, W.; Irfan, A. Rational Design of Diketopyrrolopyrrole-Based Multifunctional Materials for Organic Light-Emitting Diodes and Organic Solar Cells. *Theor. Chem. Acc.* **2018**, *137* (11), 145.

(40) Aigner, D.; Ungerböck, B.; Mayr, T.; Saf, R.; Klimant, I.; Borisov, S. M. Fluorescent Materials for pH Sensing and Imaging

https://doi.org/10.1021/acsomega.4c05710
ACS Omega 2024, 9, 42375−42385

Based on Novel 1,4-Diketopyrrolo-[3,4-C]Pyrrole Dyes. *J. Mater. Chem. C* **2013**, *1* (36), 5685−5693.
(41) Qu, Y.; Hua, J.; Tian, H. Colorimetric and Ratiometric Red Fluorescent Chemosensor for Fluoride Ion Based on Diketopyrrolopyrrole. *Org. Lett.* **2010**, *12* (15), 3320−3323.
(42) Deng, L.; Wu, W.; Guo, H.; Zhao, J.; Ji, S.; Zhang, X.; Yuan, X.; Zhang, C. Colorimetric and Ratiometric Fluorescent Chemosensor Based on Diketopyrrolopyrrole for Selective Detection of Thiols: An Experimental and Theoretical Study. *J. Org. Chem.* **2011**, *76* (22), 9294−9304.
(43) Schutting, S.; Borisov, S. M.; Klimant, I. Diketo-Pyrrolo-Pyrrole Dyes as New Colorimetric and Fluorescent pH Indicators for Optical Carbon Dioxide Sensors. *Anal. Chem.* **2013**, *85* (6), 3271−3279.
(44) Yamagata, T.; Kuwabara, J.; Kanbara, T. Synthesis of Highly Fluorescent Diketopyrrolopyrrole Derivative and Two-Step Response of Fluorescence to Acid. *Tetrahedron Lett.* **2010**, *51* (12), 1596−1599.
(45) Salyk, O.; Vyňuchal, J.; Kratochvílová, I.; Todorciuc, T.; Pavluch, J.; Toman, P. Study of Phenylpyridyldiketopyrrolopyrrole Interaction With Hydrogen in Gas and in Acids. *Phys. Status Solidi A* **2010**, *207* (10), 2327−2333.
(46) Takahashi, H.; Mizuguchi, J. Hydrogen Gas Sensor Utilizing a High Proton Affinity of Pyrrolopyrrole Derivatives. *J. Electrochem. Soc.* **2005**, *152* (6), H69.
(47) Purc, A.; Sobczyk, K.; Sakagami, Y.; Ando, A.; Kamada, K.; Gryko, D. T. Strategy Towards Large Two-Photon Absorption Cross-Sections for Diketopyrrolopyrroles. *J. Mater. Chem. C* **2015**, *3* (4), 742−749.
(48) Grzybowski, M.; Jeżewski, A.; Deperasińska, I.; Friese, D. H.; Banasiewicz, M.; Hugues, V.; Kozankiewicz, B.; Blanchard-Desce, M.; Gryko, D. T. Solvatofluorochromic, Non-centrosymmetric π-Expanded Diketopyrrolopyrrole. *Org. Biomol. Chem.* **2016**, *14* (6), 2025−2033.
(49) Podlesný, J.; Dokládalová, L.; Pytela, O.; Urbanec, A.; Klikar, M.; Almonasy, N.; Mikysek, T.; Jedryka, J.; Kityk, I. V.; Bureš, F. Structure-Property Relationships and Third-Order Nonlinearities in Diketopyrrolopyrrole Based D-π-a-π-D Molecules. *Beilstein J. Org. Chem.* **2017**, *13*, 2374−2384.
(50) Yaws, C. L. *The Yaws Handbook of Vapor Pressure: Antoine Coefficients*; Gulf Professional Publishing, 2015.
(51) Manfredi, G. Sensing With Polymer Photonic Crystals, in Organic & Hybrid Photonic Crystals for Controlling Light-Matter Interaction Processes. Ph.D. Thesis, Universtà degli Studi di Genova, 2017.
(52) Humphreys, J.; Pop, F.; Hume, P. A.; Murphy, A. S.; Lewis, W.; Davies, E. S.; Argent, S. P.; Amabilino, D. B. Solid State Structure and Properties of Phenyl Diketopyrrolopyrrole Derivatives. *CrystEngComm* **2021**, *23* (8), 1796−1814.
(53) Saes, B. W. H.; Lutz, M.; Wienk, M. M.; Meskers, S. C. J.; Janssen, R. A. J. Tuning the Optical Characteristics of Diketopyrrolopyrrole Molecules in the Solid State by Alkyl Side Chains. *J. Phys. Chem. C* **2020**, *124* (46), 25229−25238.
(54) Liu, J.; Walker, B.; Tamayo, A.; Zhang, Y.; Nguyen, T.-Q. Effects of Heteroatom Substitutions on the Crystal Structure, Film Formation, and Optoelectronic Properties of Diketopyrrolopyrrole-Based Materials. *Adv. Funct. Mater.* **2013**, *23* (1), 47−56.
(55) Hartnett, P. E.; Margulies, E. A.; Mauck, C. M.; Miller, S. A.; Wu, Y.; Wu, Y.-L.; Marks, T. J.; Wasielewski, M. R. Effects of Crystal Morphology on Singlet Exciton Fission in Diketopyrrolopyrrole Thin Films. *J. Phys. Chem. B* **2016**, *120* (7), 1357−1366.
(56) Naik, M. A.; Venkatramaiah, N.; Kanimozhi, C.; Patil, S. Influence of Side-Chain on Structural Order and Photophysical Properties in Thiophene Based Diketopyrrolopyrroles: A Systematic Study. *J. Phys. Chem. C* **2012**, *116* (50), 26128−26137.
(57) Genevaz, N.; Chávez, P.; Untilova, V.; Boeglin, A.; Bailly, C.; Karmazin, L.; Biniek, L. Tuning Crystallochromism in Diketopyrrolopyrrole-Co-thieno[3,2-B]Thiophene Derivatives by the Architecture of Their Alkyl Side Chains. *J. Mater. Chem. C* **2018**, *6* (34), 9140−9151.
(58) Mizuguchi, J.; Shikamori, H. Spectral and Crystallographic Coincidence in a Mixed Crystal of Two Components and a Crystal of Their Hybrid Component in Pyrrolopyrrole Pigments. *J. Phys. Chem. B* **2004**, *108* (7), 2154−2161.
(59) Mizuguchi, J. Correlation between Crystal and Electronic Structures in Diketopyrrolopyrrole Pigments as Viewed from Exciton Coupling Effects. *J. Phys. Chem. A* **2000**, *104* (9), 1817−1821.
(60) Mizuguchi, J.; Rihs, G. Electronic Spectra of 1,4-Diketo-3,6-Diphenyl-Pyrrolo-[3,4-c]-Pyrrole in the Solid State. *Bunsenges. Phys. Chem.* **1992**, *96* (4), 597−606.
(61) Mauck, C. M.; Hartnett, P. E.; Margulies, E. A.; Ma, L.; Miller, C. E.; Schatz, G. C.; Marks, T. J.; Wasielewski, M. R. Singlet Fission via an Excimer-Like Intermediate in 3,6-Bis(thiophen-2-yl)-diketopyrrolopyrrole Derivatives. *J. Am. Chem. Soc.* **2016**, *138* (36), 11749−11761.
(62) Law, K. Y. An Investigation of Solvent-Vapor-Induced Crystallization Soluble Vanadyl Phthalocyanine Dyes in Polymer Matrixes. *J. Phys. Chem.* **1985**, *89* (12), 2652−2657.
(63) Vaidya, S.; Johnson, C.; Wang, X.-Y.; Schmehl, R. H. Fluorescence Solvato and Vapochromism of a Dimethylaminostyryl Terpyridine Derivative. *J. Photochem. Photobiol., A* **2007**, *187* (2), 258−262.
(64) Ahmad, M.; Platonova, I.; Battisti, A.; Minei, P.; Brancato, G.; Pucci, A. Highly Selective Vapochromic Fluorescence of Polycarbonate Films Doped With an ICT-Based Solvatochromic Probe. *J. Polym. Sci., Part B: Polym. Phys.* **2017**, *55* (15), 1171−1180.
(65) Gao, S.; Tang, X.; Langner, S.; Osvet, A.; Harreiß, C.; Barr, M. K. S.; Spiecker, E.; Bachmann, J.; Brabec, C. J.; Forberich, K. Time-Resolved Analysis of Dielectric Mirrors for Vapor Sensing. *ACS Appl. Mater. Interfaces* **2018**, *10* (42), 36398−36406.
(66) Escher, A.; Alloisio, M.; Cavallo, D.; Dodero, A.; Lova, P. Beyond Labeling: Hybrid Planar Photonic Crystals for Anti-tampering Detection of Amines. *ACS Appl. Opt. Mater.* **2024**, *2* (4), 655−663.
(67) Benvenuti, E.; Lanfranchi, A.; Moschetto, S.; Natali, M.; Angelini, M.; Lova, P.; Prescimone, F.; Ragona, V.; Comoretto, D.; Prosa, M.; Bolognesi, M.; Toffanin, S. On-Chip Organic Optoelectronic System for Fluorescence Detection. *J. Mater. Chem. C* **2024**, *12* (12), 4243−4252.
(68) Liu, Z.; Chi, J.; Lian, Z.; Yang, Y.; Cheng, L.; Lin, X.; He, X.; Ji, X.; Yang, C.; Tang, Y.; Yang, M.; Gao, Z.; Gu, W.; An, H.; Wei, Q.; Song, Y.; Su, M.; Li, R.; Chai, W. Rapid Differential Diagnosis of Periprosthetic Joint Infection by Microdroplet Reaction on Portable Biochip and Indicator. *Chem. Eng. J.* **2024**, *494*, 153034.
(69) Fathi, F.; Rashidi, M.-R.; Pakchin, P. S.; Ahmadi-Kandjani, S.; Nikniazi, A. Photonic Crystal Based Biosensors: Emerging Inverse Opals for Biomarker Detection. *Talanta* **2021**, *221*, 121615.
(70) Fornasari, L.; Floris, F.; Patrini, M.; Canazza, G.; Guizzetti, G.; Comoretto, D.; Marabelli, F. Fluorescence Excitation Enhancement by Bloch Surface Wave in All-Polymer One-Dimensional Photonic Structure. *Appl. Phys. Lett.* **2014**, *105* (5), 053303.
(71) Comoretto, D. *Organic and Hybrid Photonic Crystals*, 1st ed.; Springer International Publishing: Basel, Switzerland, 2015.
(72) Zhang, X.; Qiu, J.; Li, X.; Zhao, J.; Liu, L. Complex Refractive Indices Measurements of Polymers in Visible and Near-Infrared Bands. *Appl. Opt.* **2020**, *59* (8), 2337−2344.
(73) *Gwyddion*, version 2.58; published Feb 9, 2021, http://gwyddion.net/.

https://doi.org/10.1021/acsomega.4c05710
ACS Omega 2024, 9, 42375−42385